Evaluating Shoreline Prediction Models Using Satellite Imagery and Open-Source Tools

Thomas, J.,* **Nemoto, T., Dhar, S. and Raghavan, V.**
Department of Geosciences, Osaka Metropolitan University, Japan, E-mail: sw23079s@st.omu.ac.jp*
**Corresponding Author*

DOI: https://doi.org/10.52939/ijg.v22i10.5239

Abstract
This study integrates open-source satellite-based shoreline extraction and statistical shoreline-change analysis to evaluate tidal correction and prediction ability in two contrasting coastal settings. Shoreline change is assessed using CoastSat-derived shorelines and AMBUR (Analyzing Moving Boundary Using R)-based rate modeling at Texas, United States of America and Ishikawa, Japan. Publicly available Sentinel-2, Landsat, and high-resolution elevation datasets (NOAA (National Oceanic and Atmospheric Administration) lidar, GSI (Geospatial Information Authority of Japan) DEM, and SDB (Satellite Derived Bathymetry)) are combined with hourly or model tide records to extract, tidally correct, and analyze multi-decadal shoreline positions. Validation at San Jose Island compares tidally corrected Sentinel-2 shorelines with 1 m NOAA lidar shorelines in terms of baseline distance, beach slope, and shoreline elevation. The CoastSat shoreline reproduces the lidar-derived planform with a distance RMSE of 14.26 m and 80% of transects within the low-error band; slope and elevation comparisons yield RMSE values of 3.83° and 1.05 meters, with over 78% and 85% of transects, respectively, falling within corresponding low-error thresholds. For Wajima, three different geostatistical methods were used to analyze historical Landsat shorelines from 1987 to 2014. Using 28 years of shoreline data, the 2023 pre-earthquake shoreline was extrapolated with an average error of 8.19 to 10.73 meters. The 2024 post-earthquake shoreline prediction showed errors exceeding 50 meters in MAE. Thus, when sudden shifts reshape coastlines, these trend methods fall short. Still, comparing the predicted 2023 shoreline with the observed 2024 shoreline, researchers found a coastline advance of roughly 150 to 200 meters, matching separate radar-based estimates along the Noto Peninsula. This study shows the combined CoastSat–AMBUR workflow to provides a framework for shoreline extraction, tidal correction validation, and future shoreline extrapolation and the application of CoastSat and AMBUR for before and after an earthquake.

Keywords: AMBUR, CoastSat, Open-source geospatial tools, Satellite-Derived Bathymetry (SDB), Satellite-Derived Shorelines, Shoreline Change Prediction, Tidal Correction

1. Introduction

Shoreline change refers to the alteration of coastal boundaries over time due to natural processes such as wave action, tidal currents, and sediment transport, as well as human activities including infrastructure development and land use change, and these shifts strongly affect coastal ecosystems, human settlements, and economic activities, making robust shoreline monitoring and prediction essential for management, hazard mitigation, and climate adaptation [1][2] and [3]. Recent studies have emphasized that geospatial tools such as remote sensing, GIS, and Digital Shoreline Analysis Systems (DSAS) provide a practical way to track multi-decadal shoreline evolution, delineate erosion accretion patterns, and identify high-risk zones, particularly along coasts exposed to cyclones, sea-level rise, or sediment-supply changes [2][4] and [5]. Traditional shoreline-change assessments based on field surveys or manual digitization, while valuable, are typically costly, spatially limited, and temporally inconsistent, thanks to satellite images, free software, and semi-automated systems now around, we gather data way faster and more easily. This works well for understanding past issues and making predictions too [4][5] and [6]. However, significant challenges remain: shorelines extracted from optical imagery are affected by water-level variability, wave setup, and swash, so that accurate shoreline positioning requires explicit tidal and water-level correction, careful uncertainty analysis, and, increasingly, statistical or model-based approaches that can link observed trends with future projections [6] and [7].

Against this background, the present research tackles three core problems: (i) accurate shoreline extraction from multi-sensor satellite archives, (ii) tidal correction of those shorelines using readily available elevation and bathymetric information, and (iii) prediction and validation of future shoreline positions using open-source tools in contrasting coastal environments. Specifically, the study seeks to integrate satellite-derived shorelines with statistical shoreline-change methods to assess and predict shoreline evolution under diverse geographic and environmental conditions, using two main test sites: San Jose Island, Texas, where tidally corrected CoastSat shorelines can be validated against independent observations, and Wajima, Ishikawa, Japan, where a major earthquake provides a natural experiment to examine how well pre-event shoreline behavior and model-based predictions anticipate post-event shoreline positions [6] and [7]. The proposed workflow was carried out through four main steps: (1) to integrate outputs from CoastSat, an open-source Python/GEE toolkit for shoreline extraction, and AMBUR, an R package for spatio-temporal shoreline change analysis, into a the streamlined workflow for shoreline analysis and prediction [7] and [8]; (2) to perform tidal correction on extracted shorelines using digital elevation models (DEM) and satellite-derived bathymetry (SDB) and validate their positional accuracy against reference data [6]; (3) to validate predicted shoreline positions, derived from statistical change metrics, with observed shoreline data at the study sites; and (4) to evaluate the accuracy of predicted shorelines under both pre- and post-earthquake conditions in Wajima, thereby assessing the robustness of an open-source, satellite-based workflow for application in dynamic and hazard-affected coastal settings.

2. Materials and Methods

2.1 Study Sites

Two study sites were selected to evaluate the proposed workflow under contrasting coastal conditions. as presented in Figure 1, San Jose Island was used as a relatively stable natural shoreline for validation of shoreline extraction and tidal correction, while Wajima was selected as a hazard-affected site to examine workflow performance under pre- and post-earthquake shoreline change.

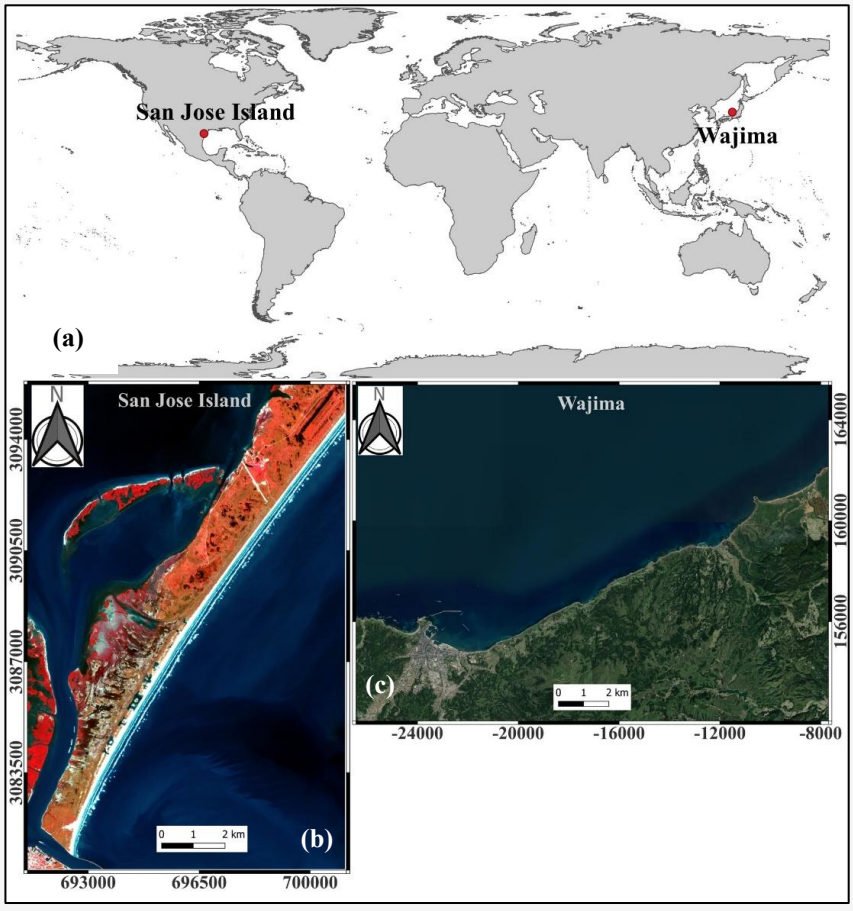

Figure 1: Study areas: (a) Location of two sites (b) San Jose Island, Texas, USA (c) Wajima, Ishikawa, Japan

San Jose Island, which is also known as Saint Joseph Island, is a barrier island located on the Gulf Coast of Texas, where the length of the island is approximately around 34 kilometers in length and 8 kilometers in width but the area of interest for this study was 15.7 kilometers. Geographically, it is situated at latitude 28°00′18" N and longitude 96°56′02" W, as displayed in Figure 1(b). For San Jose, studies show that the vegetation and shoreline change along other segments of Texas Gulf Coast are present due to the result of natural process [9]. This is a good study site to perform the validation, as there is less contamination by beach nourishment, seawalls, and other human interventions. The study area Wajima is located on Noto Peninsula in Ishikawa prefecture Japan as showed in Figure 1(c); it is situated geographically at latitude 37°23′27.24" N and longitude 136°53′58.562" E. The region experienced an earthquake of 7.6 magnitude [10] on 1st January 2024 and because of this it is seismically active. Because of this event, there was damage around Wajima and its surrounding areas, the events occurred including tsunami and crustal deformation also resulting landslides, inundation and destruction of infrastructures. Hence understanding and extrapolating future shoreline change will be crucial for disasters preparedness and coastal management.

2.2 Data Collection and Preparation

This study consists of two distinct coastal regions: San Jose Island and Wajima (Table 1). For both area datasets were compiled to facilitate shoreline analysis using the CoastSat and AMBUR tools.

2.2.1 Data used for San Jose Island

The shoreline dynamics analysis done for San Jose Island consists of multiple datasets, which were utilized to ensure accurate assessments (Table 1). Sentinel-2 mission with high-resolution satellite imagery was obtained for the year 2018 and then shorelines were extracted and tidal correction was also performed on the shorelines. These images were retrieved using CoastSat toolkit, which enables the extraction of shoreline positions from satellite data that are publicly available [7]**.** To account for tidal influences on the shorelines, tidal data were sourced from the National Oceanic and Atmospheric Administration (NOAA) Tides and Currents database, which provided measurements with one-hour temporal resolution. Additionally, to calculate beach slope and shoreline elevation, from NOAA's Data Access Viewer [11] Light Detection and Ranging (LiDAR) data were acquired**.** The LiDAR-derived Digital Elevation Model (DEM) has a spatial resolution of 1 meter providing topographic information essential to understand and conduct accurate shoreline analysis. The integration of Sentinel-2 imagery, tidal records, and LiDAR DEM can be used for extracting detailed shorelines and performing tidal corrections.

2.2.2 Data used for Wajima, Ishikawa

To analyze the changes occurring at the shoreline and predict future shorelines, a data set of 28 years has been collected for this analysis, which covers the following years: 1987-2014, 2018, 2023 and 2024 (Refer to Table 1). The position of the shoreline has been determined using satellite imagery captured by Landsat 5 TM, Landsat 7 ETM+ and Landsat 8 OLI. The bands used include RGB, NIR, and SWIR, which had an initial resolution of 30 meters, which has now been increased to 15 meters. Tidal data is essential for accurate shoreline positioning, and in this study the tide data was sourced from the Geospatial Information Authority of Japan (GSI) [12]. There are many networks of tide station network across Japan, which is operated by GSI, providing hourly tidal height data which can be used for performing precise tide corrections corresponding to the satellite imagery acquisition times. The Wajima tide station is located at latitude 37°23′30" N and longitude 136°54′00" E, the tide station has been operated since 1952, offering a long-term record of tidal observations. The GSI of Japan provides DEM with a spatial resolution of five meters, which was derived from photogrammetric method, giving a detailed elevation information essential for understanding costal morphology of the shorelines. Along with it, bathymetry data was also obtained from General Bathymetric Chart of the Oceans (GEBCO), that provides bathymetric DEM with a spatial resolution of 500 meters.

2.3 Analysis Method at San Jose Island

For this study site, the analysis was done by CoastSat, which is a python toolkit designed to extract shorelines from publicly available satellite imagery, facilitating large-scale coastal monitoring [7]. The methodology begins with the acquisition of satellite images, primarily from Landsat and Sentinel missions, which provide extensive temporal coverage. These images undergo preprocessing steps, including cloud masking to enhance the quality. The toolkit also employs a supervised classification approach to distinguish between land and water pixels, that helps in the delineation of the shorelines. The extracted shorelines are then subjected to a tidal correction process, to adjust the position. The detailed structure can be seen in Figure 2.

Table 1: Data source for San Jose and Wajima

Study Area	Data	Year	Data Collection	Resolution
San Jose Island	Sentinel 2	2018	CoastSat	10 (m) *
San Jose Island	LiDAR DEM	2018	NOAA	1 (m) *
San Jose Island	Tide Data	2018	NOAA	15-60 minutes **
Wajima	Landsat 5 TM	1987-1998, 2004-2011	CoastSat	15 (m) *
Wajima	Landsat 7 ETM	1999-2003	CoastSat	15 (m) *
Wajima	Landsat 8 OLI	2013-2014, 2018, 2023, 2024	CoastSat	15 (m) *
Wajima	Photogrammetry DEM	2018	GSI	5 (m) *
Wajima	Bathymetry	2023	GEBCO	500 (m) *
Wajima,	Tide Data	1987-2014	GSI	15-60 minutes**

*Note: * Spatial Resolution, **Temporal Resolution*

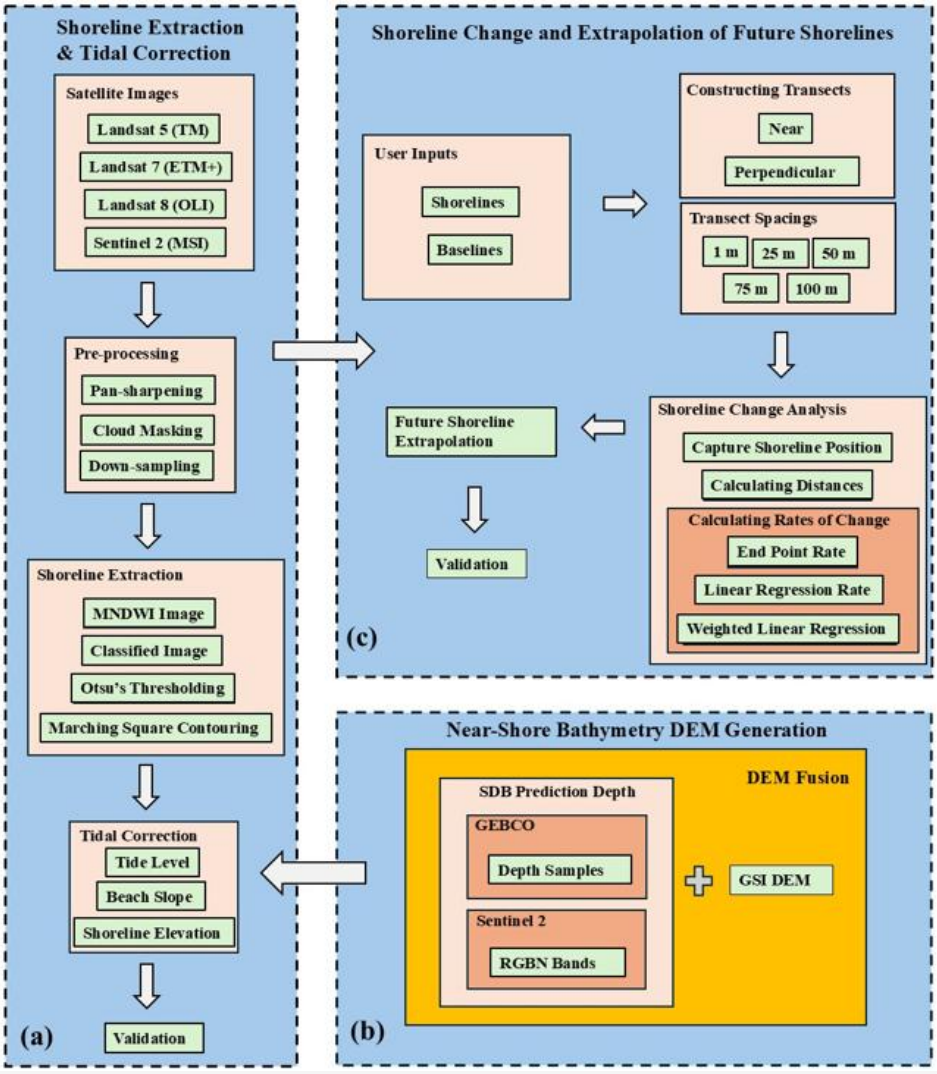

Figure 2: Workflow: (a) Shoreline extraction & tidal correction (b) Bathymetry generation (c) Calculating shoreline change rate & future shoreline extrapolation

2.3.1 Shoreline extraction

Figure 2(a) shows shoreline extraction process integrates satellite imagery acquisition, preprocessing, and segmentation techniques to delineate coastal boundaries accurately and the retrieval of satellite images from platform such as Landsat 5, 7, 8 and Sentinel 2 were performed using Google Earth Engine (GEE), later preprocessing such as cloud masking, pan-sharpening and down-sampling techniques were applied to improve spatial resolution. Following pre-processing, the Modified Normalized Difference Water Index (MNDWI) is computed to distinguish water bodies from land areas. The MNDWI is calculated using Green and Shortwave Infrared (SWIR) bands of satellite imagery, as defined by [13] in Equation 1:

$$MNDWI = \frac{SWIR - Green}{SWIR + Green}$$

Equation 1

Where:

$MNDWI$ = Modified Normalized Difference Water Index,
$SWIR$ = Shortwave Infrared band,
$Green$ = Green band

This index enhances the presence of water features and suppresses the noise from built-up land features, soil and vegetation. Otsu's thresholding method is employed, to separate water and non-water regions within the MNDWI. Otsu's thresholding technique determines an optimal threshold value by maximizing between class variance from the histogram of the MNDWI values, effectively binarizing the image into water and non-water classes [14]. Once the binary image is obtained, then the shorelines are delineated by identifying the boundary line between the water and land pixels. This is achieved at sub-pixel level resolution by applying the Marching Squares Algorithm [15] and [16]. By integrating the methods MNDWI, Otsu's thresholding and Marching Squares Algorithm gives the accurate extraction of shorelines from satellite imagery, giving essential data that can be used for coastal management and monitoring.

2.3.2 Tidal correction

The tidal correction technique plays a very vital role in the process of standardization of the location of shorelines obtained from the satellite images to the same tidal datum level, which is usually the MSL (Mean Sea Level). The shorelines obtained from satellite images are recorded under different levels of tides; therefore, tidal correction is very important. For this study, Figure 2(a) shows the process of tidal correction, that begins with the extraction of shorelines from satellites images, each associated with a specific acquisition time. To determine the corresponding tidal level with respect to the time of image acquisition, the global tide model Finite Element Solution 2022 (FES2022) [17] was utilized. In contrast, for San Jose Island observed tidal data from authoritative source, NOAA Currents and Tides, these provides high-quality tidal data, ensuring precise tidal corrections. Once the tidal levels corresponding to each satellite image is obtained, the next step involves estimating beach-face slope (m). In this study the beach-face slope is estimated by calculating slopes from the DEM using Horn's algorithm [18] and then overlaying the extracted shoreline points with 1-meter intervals between the points, based on the resolution of DEM and the slope values were extracted, and then the average slope values were used further for performing the tidal correction. An experiment was conducted in [19], where low slopes, average slope, and high slope values were used separately for tidal correction and among them the average slope gave low errors. The reference elevation z_{ref} were also extracted by overlaying the shoreline points on DEM and then extracting the mean shoreline elevation, which is applied at the points where user defined transect intersect with the shorelines. Previous DEM based workflow for tidal correction have also used high-resolution DEM to derive slope for tidal normalization of satellite derived shorelines. For example [20], compute cross-shore slopes along transects from one meter DEM and then perform a linear correction using the ratio between tidal height difference and local slope. In contrast to this method, our study also derives shoreline reference elevation directly from one meter DEM and uses this elevation in the correction equation.

Each of the satellite image captures the shoreline at a distinct tidal phase, it's essential to apply a linear tidal correction. The correction performed utilizes observed tide levels and the characteristic of the beach face to adjust each shoreline position to a standard reference elevation [7]. The formula for tidal correction is expressed below (Equation 2):

$$\Delta x = \frac{z_{ref} - z_{wl}}{m}$$

Equation 2

Where:

Δx = Cross-shore horizontal shift
z_{ref} = Reference elevation
z_{ref} = Local tide level,
m = Beach slope

2.4 Analysis Method at Wajima

In this site, 2 open-source tools were used, CoastSat and AMBUR. CoastSat was used for shoreline extraction, and tidal correction, AMBUR tool was used for analyzing shoreline change over time and extrapolate future shoreline where it uses GIS techniques and geo-statistical methods. For this the inputs required are onshore and offshore baselines and shorelines. These shorelines are extracted from satellite images and tidally corrected using CoastSat. From these baselines, transects are drawn at user-defined intervals to intersect shorelines at specific points, allowing for precise measurements of shoreline movement [8].

2.4.1 Methodology for high-resolution nearshore bathymetry generation

This study used the DEM from GSI with five meters spatial resolution, since the DEM was generated using photogrammetry techniques, it only generated the topography of land features, whereas the bathymetry is also important, as most of the shorelines are falling outside the DEM. Hence bathymetry DEM is essential for performing tidal correction. The generation of the bathymetry was conducted using Satellite-Derived Bathymetry (SDB) technique, using Sentinel-2 imagery. This method involves extracting depth values from optical satellite images, which were calibrated using depth samples. These samples were derived from GEBCO datasets, to ensure accuracy in shallow water regions. The SDB process was executed using the SDB GUI tool developed by [21].

After generating the SDB, to improve the bathymetry DEM, SDB-derived bathymetry was fussed with the GSI terrestrial DEM, ensuring a seamless transition between land and underwater topography. This integration enhanced the precision of nearshore topography. The final high-resolution bathymetry DEM was used further to calculate beach-slope and shoreline elevation for performing tidal correction on shorelines as it was done for San Jose Island as displayed in Figure 2(b).

2.4.2 Shoreline extraction and tidal correction

Shoreline extraction process and the tidal correction applied at Wajima is same method that was used for San Jose Island, the only difference is the DEM used for this study site. The DEM used for tidal correction was the fusion of SDB and GSI DEM, where slope and shoreline elevation was estimated (refer Figure 2(a) and 2(b)). The tide data used in this site was from GSI, the tidal correction was performed using Equation 2.

2.4.3 AMBUR-based shoreline analysis

AMBUR calculates shoreline change rates using methods such as the End Point Rate (EPR), where it divides the distance between the new and the oldest shoreline positions by the time elapsed. The Linear Regression Rate (LRR) fits a regression line to all the shoreline positions for each transect, providing rate of change. In weighted Linear Regression (WLR) method weights are assigned to shoreline positions based on data accuracy and time intervals, offering a refined calculation [22].

2.4.4 Transect generation

The AMBUR package assists systematic shoreline change analysis through transect generation, a fundamental process for quantifying shoreline movement over time, hence this is one of the important steps. By establishing a series of transect lines from a baseline to intersect shorelines at specific intervals, researchers can systematically measure the change in the shoreline positions. This method facilitates the calculation of rates of change, aiding in the analysis of coastal dynamics and informing management decisions [23].

In shoreline analysis, there are two methods for transect generation: perpendicular and near transects. The perpendicular transect method is performed using a baseline, which is typically positioned either offshore or onshore relative to the historical shorelines. The baseline and perpendicular transect method were introduced by [8], which is effective for relatively linear shorelines. This may present challenges when applied to curved or irregular shorelines, as the perpendicular transect might not accurately represent the true orientation of shoreline change [8]. To address the limitation of the perpendicular method, AMBUR also included the near transect approach. This method is advantageous for analyzing curved complex shorelines, the near method generates transect by identifying the nearest points along the shoreline, which allows more accurate representation of shoreline dynamics, mainly in those areas where the perpendicular method may be less effective [8]. For this site, five different near transects were generated at intervals of 1, 25, 50, 75 and 100 meters. This allows us to compare the shoreline movement with different spatial resolutions. The one-meter intervals capture fine-scale shoreline movement, while the 100 meters interval provides more generalized view of the shoreline progress.

2.4.5 Statistical method for estimating shoreline change rate

The statistical methods for shoreline change rate analysis are EPR, LRR and WLR, which are essential in coastal geomorphology, that enables researchers to quantify and assess shoreline dynamics. These methods were initially developed by previous study [22] and later included into the AMBUR package [8], providing a systematic approach to measure shoreline evolution. The EPR is widely used and a simple method which calculates the rates of change by dividing the total change in shoreline position by the time elapsed between the earliest and the most recent shoreline measurements. From Equation 3, D_f and D_i represent the shoreline positions at the final and initial time points and $T_f - T_i$ denotes the time span between the two measurements. The primary advantage of EPR is its ease of computation, but it does not account for intermediate shoreline changes, making it susceptible to temporal variability and outliers [22] as shown in Equation 3:

$$EPR = \frac{D_f - D_i}{T_f - T_i}$$

Equation 3

The LRR equation is a better version of EPR by incorporating all shoreline data points over time. Least-square regression analysis is performed over the datasets to fit a linear trend, and the regression equation is shown in Equation 4:

$$LRR = \frac{\sum_{i=1}^{n}(x_i - \bar{x})(y_i - \bar{y})}{\sum_{i=1}^{n}(x_i - \bar{x})^2}$$

Equation 4

Where:

n = number of data points (years and distances)

x_i and y_i = individual year and corresponding shoreline position measurement

$\bar{x}$ and $\bar{y}$ = mean of x_i and y_i, respectively

When estimating the shoreline change rate using LRR, it minimizes the influence of short-term variabilities, making it more comprehensive and statistically robust [22]. The shoreline change rates may not always show actual coastal dynamics, because for LRR it assumes shoreline movements in a linear trend. To address the issues of LRR, WLR was introduced, the only difference is the weights are assigned to shoreline positions based on factors like data accuracy and temporal accuracy. The weighted regression is expressed in Equation 5:

$$WLR = \frac{\sum_{i=1}^{n} w_i (x_i - \bar{x})(y_i - \bar{y})}{\sum_{i=1}^{n} w_i (x_i - \bar{x})^2}$$

Equation 5

Where w_i = assigned weight as uncertainty values

The AMBUR package, developed by [8], integrates Equation 3,4 and 5 in a GIS-based framework, for efficient shoreline analysis.

2.4.6 Future shoreline extrapolation

The extrapolation of future shorelines mainly depends on the historical shoreline change rates to predict the shorelines point providing insights that can be useful for coastal management and hazard mitigation [24]. The AMBUR package has many functions, and among them there is ambur.forecast function, which provides users to project future shoreline positions by extrapolating historical shoreline change rate at each transect. This generates a new shapefile with polyline of the forecasted shoreline in it. Currently, the extrapolation method used in AMBUR uses the linear extrapolation from the statistical methods EPR, LRR and WLR rates as shown in Figure 2(c). While this approach is employed by researchers e.g., [25], there are no standard methods for prediction or forecasting of shorelines positions across all shoreline environments. While the techniques of linear regression can be simple and useful for linear forecasting, including the linear and non-linear statistical methods have also shown to be equally reliable for predicting the future trends [24]. Recently, [26][27] and [28], proposed new shoreline forecasting techniques and compared the reliability when applied to select Hawaiian shorelines. In AMBUR package, the programming code obtained from the author of those studies is converted from MATLAB into R code along with the methods found in previously published and unpublished research.

3. Result and Discussion

3.1 Tidal Correction and Validation – San Jose Island, Texas

In San Jose Island, the tidal correction was performed using the CoasSat tool on satellite derived shorelines from 2018. The reference shoreline used for validation was extracted from Lidar and ortho-images collected for the same period by NOAA Coastal Mapping Program [11].

The validation performed involved three key metrics: Distribution of distances, beach-slope, and elevation differences between tidally corrected and reference shorelines. A similar multi-metric framework has been applied to compare satellite-derived shorelines with traditionally sourced lidar and field shorelines across diverse U.S. coastal settings [20].

3.1.1 Distance comparison between CoastSat and NOAA shorelines

To perform the validation of the tidal correction using distance, 3 data were used, which are baseline, tidally corrected shoreline and reference shoreline. The distances were calculated from tidally corrected shoreline to the baseline and the same was done for the reference shoreline. Using a shared baseline and comparing shoreline-normal distances is a standard approach for assessing positional agreement between satellite-derived and traditional shoreline datasets [20]. For distances, 2 plots were calculated, an overlay plot and a signed difference plot. In the Figure 3(a), the overlay of baseline distances shows the comparison of 1m NOAA lidar-derived shoreline and the 10m Sentinel-2 shoreline along San Jose Island, from north (Transect ID 1072) to south (Transect ID 16290). The two distance curves have similar peaks, low-error zones cover 80.03% of the whole area. In the northern third of the island (approximately Transect IDs 1072 - 4300), the overlay of baseline distances shows both shorelines follow nearly along shore trend, this can also be observed between 6200 – 7200, 13000, and 15000 transect IDs. Moving southward into the middle section of the transect IDs 8000 - 11000, the two curves track the same broad inlet and bulge, but the systematic seaward displacement of the CoastSat shorelines become more apparent. The overall RMSE of 14.26 then indicates that the CoastSat shoreline reproduces the outlier of the lidar shoreline to within roughly one pixel to one and a half pixel, this shows the accurate shoreline extraction and tidal correction. Comparable-scale differences between satellite-derived and traditionally sourced shorelines have been reported in other coastal environments, indicating that RMSE values on the order of one to a few pixels are consistent with useful cross-method agreement [20]. In signed difference plot as displayed in Figure 3(b), the mean signed distances difference is +8.75 m, confirming the CoastSat shoreline is, on average, nearly 9 m farther than the NOAA shoreline. The residuals ranging from negative 8.17 m to positive 41.85 m, where the negative residuals show CoastSat is closer than NOAA and positive residuals represent CoastSat tends to be seaward. The largest discrepancies occur in a central-southern reach (approximately transect IDs 8000-11000), where residuals form a broad plateau of positive values up to about +41.85 m. These areas likely agree with morphological distinct zones with lower slopes or more energetic wave conditions, where the rapid shoreline proxy diverges from the datum-based shoreline even after tidal correction.

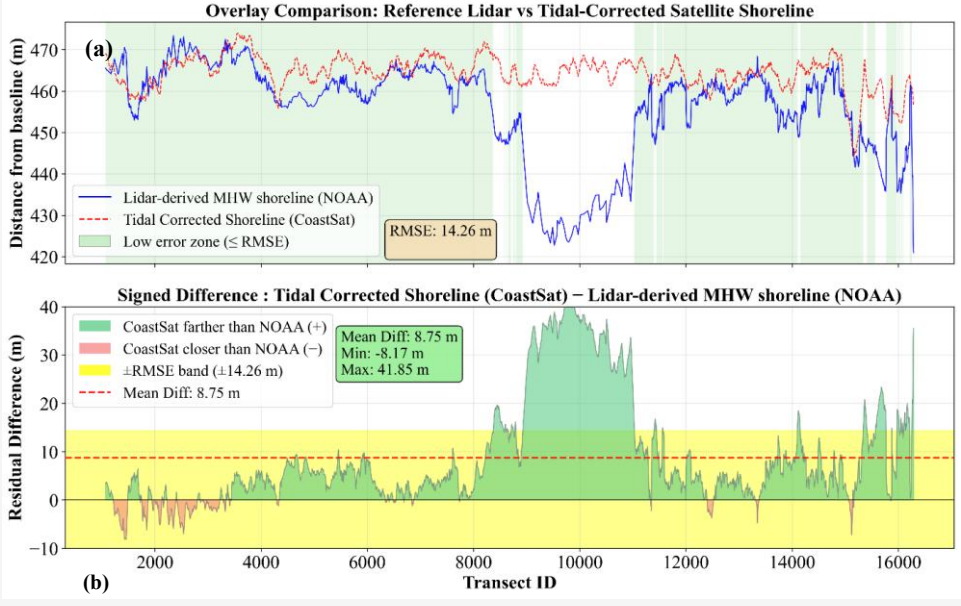

Figure 3: Tidal correction validation result of distance-based comparison between NOAA shoreline and CoastSat shoreline: (a) Overlay Comparison and (b) Signed Difference

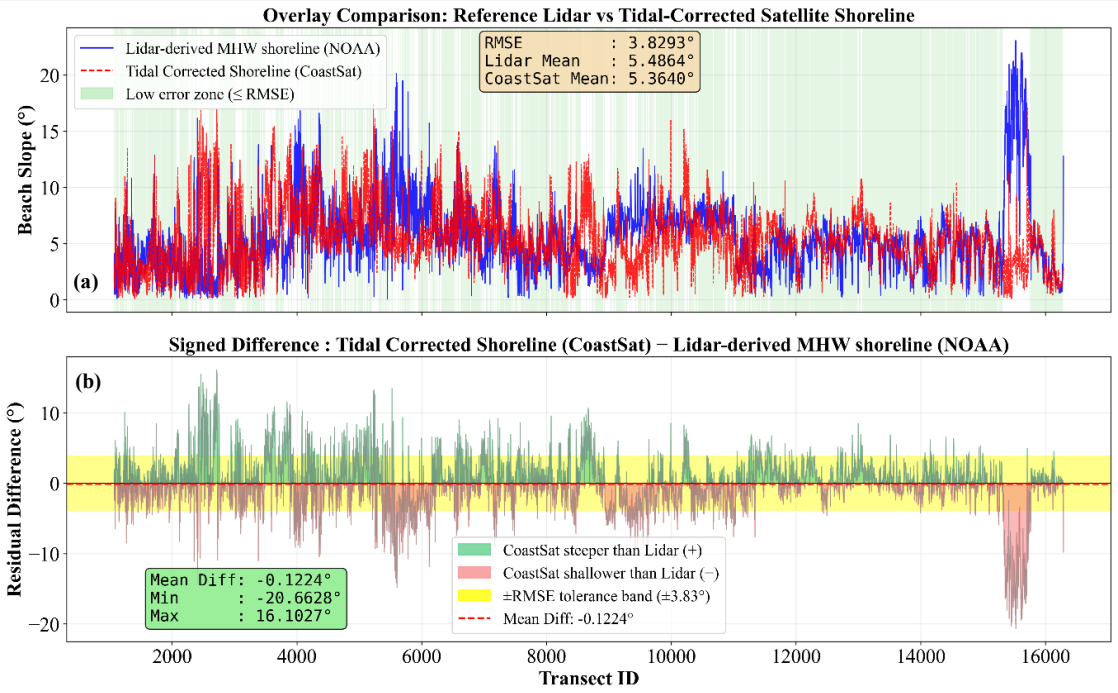

Figure 4: Tidal correction validation result of beach-slope-based comparison between NOAA Shoreline and CoastSat shoreline: (a) Overlay Comparison (b) Signed Difference

3.1.2 Beach-Slope comparison

The beach-slope validation compares 1 m NOAA lidar extracted shoreline slope with slopes extracted from tidally corrected 10 m Sentinel-2 CoastSat shorelines along San Jose Island, where the transect ID 1072 in the north to 16290 in the south. In the overlay plot, both the datasets show similar alongshore variations in slope, indicating that CoastSat captures the main transitions between gentler and steeper slope sections of the beach face. The overall RMSE between NOAA and CoastSat slopes is 3.83°, with mean slopes of 5.49° for NOAA and 5.36° for CoastSat, and a mean difference of -0.12° throughout the whole island. 78.59% of the island falls under the "low error" band where the absolute slope difference is ≤3.83°, highlighted by the green shading. These low error zones correspond mainly to the long, relatively uniform open-coast segments in the northern and the central parts of the island, where the two slope curves lie closely together for thousands of consecutives transects as shown in Figure 4(a). The Signed-difference plot with CoastSat and NOAA, shows how slope changes alongshore and whether CoastSat is steeper or flatter than NOAA's shoreline. The residuals that are around zero, confirming the small overall bias, but the individual transect shows a wide range from -20.66° showing CoastSat slopes are much flatter up to +16.10° showing CoastSat much steeper. Most of the transects lie within the RMSE tolerance band of ±3.83° (yellow), (refer to Figure 4(b)) where discrepancies are modest after the tidal corrections. The overall statistic indicates that CoastSat provides a realistic estimate of beach slope at San Jose Island, with good agreement over extensive alongshore distances and only a small net bias.

3.1.3 Elevation comparison

Along San Jose Island, the comparison of 1 m NOAA shoreline and 10 m Sentinel-2 CoastSat shoreline shows the satellite derived tidally corrected shorelines tracks the NOAA shoreline elevation, but with a vertical offset around transect 9000 – 11000. In the overlay plot, both profiles rise and fall together from north (Transect ID 1072) to south (Transect ID 16290): where the NOAA based shorelines elevation gently increases or decreases, CoastSat also follows the same pattern, indicating the tidal correction responding to the same morphology of the NOAA shoreline as shown in Figure 5(a). With the RMSE of 1.05 m, the low error zones lie within the RMSE range where they almost cover 85% of the island, showing CoastSat elevation stays within about 1m of the NOAA, indicating that the tidal correction performed on CoastSat successfully place it close to the NOAA shoreline. The main change occurs in the central part of the island between transect IDs 9000 – 11000, where the NOAA shoreline shows a high elevation hump, this shows that in this part the NOAA shoreline stays at the steeper upper beach and

dune terrain; the CoastSat fails to reproduce the full increase in elevation after the tidal correction in this part of the transect. The signed-difference plot offers a compact view of the patterns by showing the differences between the elevations of CoastSat and NOAA derived shorelines. The differences are mostly negative, with a mean around -0.64 m and most values in the northern and southern segments fall within the RMSE band roughly ±1.05 m, which shows the vertical errors in the order of meter or less and low bias alongshore in the low-error zones. The signed differences around the central part of the island from transect 9000 – 11000, shows a block of strong negative residuals where CoastSat is lower than the NOAA shorelines (Figure 5(b)). All three metrics show that after the tidal correction on CoastSat derived shorelines reproduce the main alongshore morphology of the NOAA lidar derived shorelines. This pattern, where tidally corrected satellite shorelines reproduce the main alongshore morphology of lidar-derived shorelines with localized discrepancies in complex or steep sections, is consistent with findings from Satellite-derived shorelines (SDS) traditional shoreline comparison studies in other regions [20]. There are few discrepancies in the metrics of elevation and distances in central part of the island, this is because of how the shorelines were extracted from NOAA lidar derived shorelines or one other reason is the tidal correction performed on the CoastSat shoreline. The tidal correction performed on CoastSat was not applied to each transect, as it was performed on the entire shoreline.

3.2 Pre- and Post-Earthquake Prediction at Wajima, Japan

3.2.1 Pre-Earthquake shoreline prediction for 2023

The pre-earthquake shoreline positions for Wajima, Japan, (2023) were predicted from historical shoreline positions of 28 years (1987 – 2014) and their shoreline change rates. Shoreline change rates obtained from statistical analysis using the EPR, WLR, and LRR models were extrapolated to predict future shoreline changes. The prediction of the future shoreline positions was validated with observed shorelines extracted from satellite images using the CoastSat model. This was achieved by calculating MAE and standard deviation between the observed and predicted shorelines as shown in Table 2, Table 3, and Table 4. Method EPR showed the highest error of MAE between 9.69 m and 10.73 m, with standard deviation varying from 10.94 m to 12.71 m at different transect intervals of 1 m, 25 m, 50 m, 75 m and 100 m. 1 m interval was the transect interval with the lowest error with an MAE of 9.69 m while 100 m was the interval with the highest error. WLR method showed a lower MAE of between 8.67 m to 10.15 m while standard deviation ranged between 11.02 m to 12.70 m. 1 meter transect interval was again the interval with the lowest error with a margin of 8.67 m. From all three methods, LRR had the highest predictive accuracy, showing MAEs between 8.19 m and 9.68 m, as well as a standard deviation between 10.69 m and 12.32 m. In this case, the most accurate results were produced by the one-meter distance with an MAE value of 8.19 m.

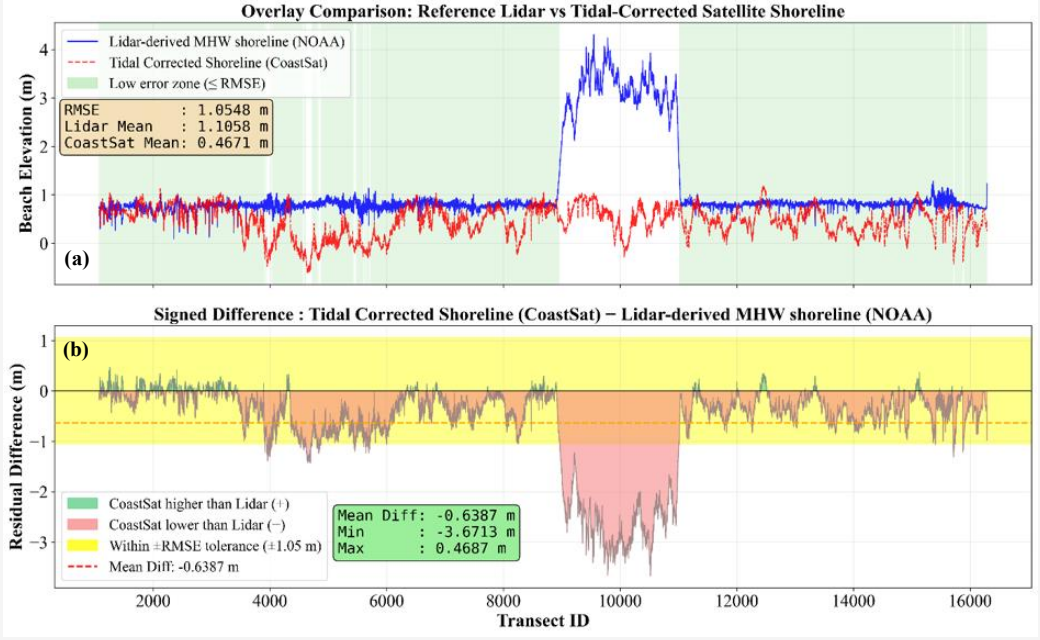

Figure 5: Tidal correction validation result of elevation-based comparison between NOAA Shoreline and CoastSat shoreline: (a) Overlay Comparison and (b) Signed Difference

Table 2: Pre-Earthquake shoreline prediction for 2023 using EPR in Wajima

Distance Interval (m)	Transect Method	Standard Deviation (m)	Mean Absolute Error (m)
1	Near	12.71	9.69
25	Near	11.61	9.71
50	Near	10.94	9.73
75	Near	11.62	10.33
100	Near	11.93	10.73

Table 3: Pre-earthquake shoreline prediction for 2023 using LRR in Wajima

Distance Interval (m)	Transect Method	Standard Deviation (m)	Mean Absolute Error (m)
1	Near	12.31	8.19
25	Near	11.12	8.21
50	Near	10.69	8.49
75	Near	11.59	9.01
100	Near	12.32	9.68

Table 4: Pre-Earthquake Shoreline Prediction for 2023 Using WLR in Wajima

Distance Interval (m)	Transect Method	Standard Deviation (m)	Mean Absolute Error (m)
1	Near	12.62	8.67
25	Near	11.45	8.70
50	Near	11.02	8.98
75	Near	11.91	9.49
100	Near	12.70	10.15

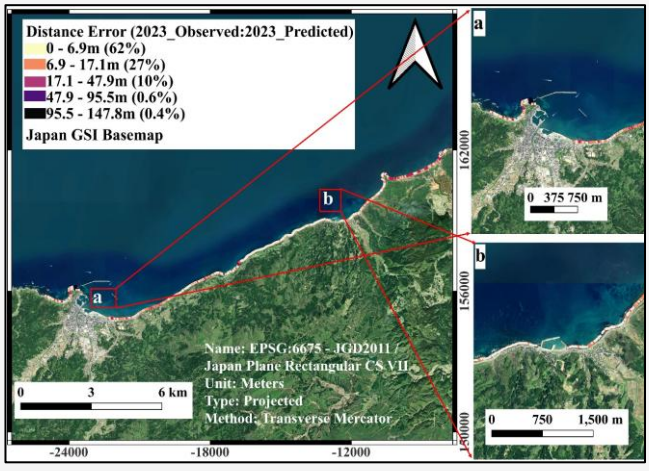

Figure 6: Distance error map for 2023 Wajima & Nafune

This finding can be interpreted as better predictive ability at the finer scale shoreline. In this experiment, the shoreline was extracted using Landsat satellite imagery of 15 meters resolution. The obtained accuracy of 8.19 m, which is less than the size of one pixel, indicates sub-pixel accuracy. Errors in spatial shoreline prediction are displayed in Figure 6 in terms of colored strips showing various ranges of errors. 62% of predictions showed errors below 6.90 m, while 27% occurred in a wider band from 6.90 m to 17.10 m. No more than 0.4% of predictions exceeded 95.50 m error value. This shows high predictive accuracy of LLR shoreline prediction for 2023 Another illustration of the predictive ability of the LRR model for the pre-earthquake shoreline in 2023 is shown in the scatter plot of predicted vs. observed distances (Figure 7). It shows that the predicted values coincide with observations almost perfectly since points cluster around the 1:1 line regardless of the distance from the baseline. Indeed,

it can be seen from the coefficient of determination $R^2 = 0.904$ that the variability of the observations is well captured by the predictions made with LRR since roughly 90% of the total variance in the observed shoreline position is accounted for, and the residual error equals just 23.0 m. The deviations from the 1:1 line occur only for some transects; hence, they can be considered a result of the local deviation from the long-term linear tendency rather than the biased results obtained via the modelling technique.

3.2.2 Post-Earthquake shoreline prediction for 2024

However, the discrepancies between the predicted and actual shorelines are quite large, especially for year 2024 since the effect of the quake on the coastline is accounted for in the observed shoreline and yet not included in the predicted one in year 2024. The MAEs for the various methods ranged for each statistical approach and distance between transects used in estimating shoreline positions. The method with the largest errors, among the three approaches tested, was EPR method, whose maximum MAE value reached 55.07 meters for one meter distance between transects. The MAE values for all methods did not change very much with the distance between transects ranging from 55.19 meters at 25 meters, 54.94 meters at 50 meters to 54.97 meters at 75 meters (Table 5). 54.13 m was the lowest MAE was recorded at 100 meters transect interval, showing very slight decrease in error at larger intervals but it is not so much of a difference. For the WLR approach, the minimum MAE obtained was 53.6 m at the 100 meters interval as shown in Table 6. Standard deviations in all methods varied from 41.33 m for WLR (at 100 meters interval) to 44.69 m for EPR (at one meter interval). From the standard deviations, it can be observed that the predicted shoreline values had high variations. It confirms the observation that the model did not consider the sudden geomorphological changes associated with the earthquake event (Table 5 and Table 6). From the map showing the distribution of the shoreline predictions error, it is evident that 35 percent of the shoreline shifts were less than 27.1 meters, while 24 percent were between 27.10 and 57.5 0m, 20 percent between 57.50 and 88.80 m, 13 percent between 88.80 and 121.70 m, and 8 percent above 121.70 m, as illustrated in Figure 8. Figure 9 Shows the Validation of the WLR model, which involves comparison of modeled shoreline positions with the observed shoreline positions in 2024 based on 100 m transect spacing in Wajima.

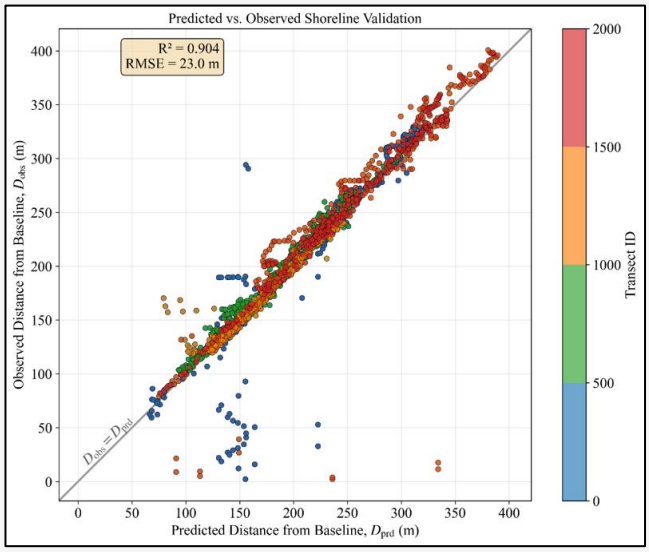

Figure 7: Predicted vs observed shoreline validation for 2023

Table 5: Post-earthquake shoreline prediction for 2024 using EPR in Wajima

Distance Interval (m)	Transect Method	Standard Deviation (m)	Mean Absolute Error (m)
1	Near	44.69	55.07
25	Near	44.33	55.19
50	Near	43.85	54.94
75	Near	44.04	54.97
100	Near	41.81	54.13

Table 6: Post-earthquake shoreline prediction for 2024 using WLR in Wajima

Distance Interval (m)	Transect Method	Standard Deviation (m)	Mean Absolute Error (m)
1	Near	42.72	54.18
25	Near	42.41	54.30
50	Near	42.19	54.08
75	Near	42.28	54.15
100	Near	41.33	53.60

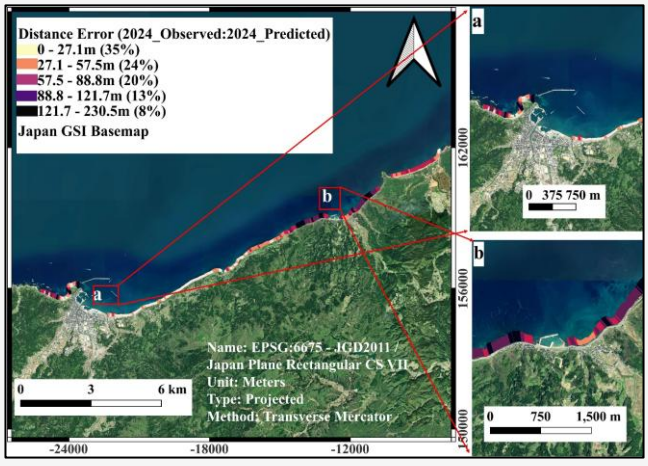

Figure 8: Distance error map for 2024 Wajima & Nafune

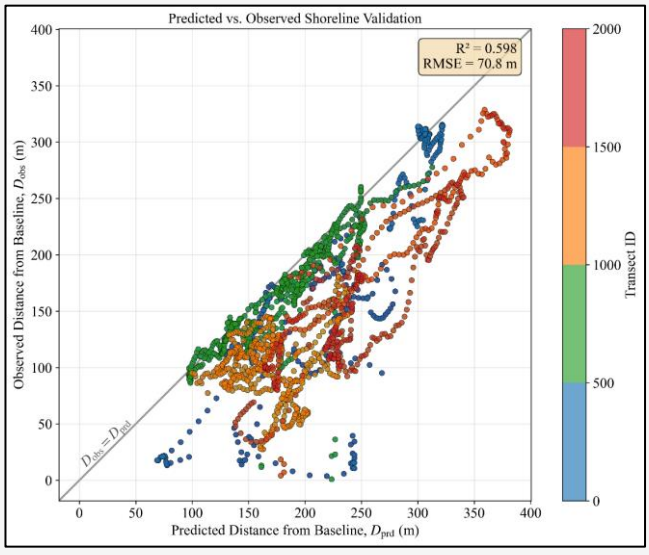

Figure 9: Predicted vs observed shoreline validation for 2024

From Figure 9, only few points fall close to the 1:1 line implying that the WLR model cannot predict accurately. The R-squared value of 0.598 implies that there is about 60% variation explained by the prediction, thus showing that it predicted very fairly. An overall root mean square error of 70.8 m suggests discrepancies, which is reasonably not good for estimating shoreline change, this is because pre-earthquake behavior and cannot capture the sudden, spatially variable shoreline shifts caused by seismic uplift/subsidence, sediment redistribution, and post-event morphodynamical adjustment. In other words, the poor statistical performance here is evidence that shoreline prediction methods derived from historical trends break down when a major tectonic disturbance fundamentally alters the coastal morphology. The limitations of the post-earthquake predictions are clearly illustrated by the WLR validation scatter plot for 2024 (Figure 9). Unlike the tight clustering around the 1:1 line obtained for 2023,

the 2024 points form broad, diverging clouds, with only a small subset lying close to the 1:1 line. The coefficient of determination is modest ($R^2 = 0.598$), indicating that roughly 40% of the variance in observed shoreline position is not explained by the model, while the RMSE of 70.8 m confirms large typical discrepancies, far exceeding the image pixel size resolution.

Systematic offsets for groups of transects, rather than random scatter, reveal spatially coherent misfits that are consistent with seismic uplift, subsidence, and subsequent morphodynamical adjustment that are absent from the regression-based trend model. In combination with the large MAE values, this plot demonstrates that pre-event statistical extrapolation is inadequate for forecasting shoreline positions after the 2024 Noto Peninsula Earthquake.

3.2.2 Shoreline change at Wajima before andaAfter the 2024 Noto Peninsula earthquake

Two shorelines were compared: predicted for 10 August 2023 and extracted for 6 April 2024. The 2023 pre-earthquake shoreline was predicted with the help of AMBUR, by using 28 years of shorelines from 1987-2014 to calculate the shoreline-change rates at Wajima and Nafune by EPR, WLR and LRR methods. Where LRR provided the most accurate result (Figure 6 and Figure 7), with MAE values of 8.19–9.68 m (Table 6) at 1 m transect spacing, which smaller than the 15 m Landsat pixel size and therefore indicates sub-pixel predictive skill for the 2023 shoreline baseline. For 2024, the shoreline was then extracted independently with CoastSat, and the horizontal shoreline shift between 2023 (predicted) and 2024 (observed) was computed. The drone-image maps for Wajima and Nafune highlight contiguous red and orange segments where the shoreline advanced seaward by approximately 150–200 m as seen in Figure 10(c) and Figure 11(c), with smaller green segments indicating limited change of less than about 40 m. These results are consistent with the SAR-based analyses by GSI report [12] as displayed in Figure 10(b) and Figure 11(b), which report seismic coastal uplift along roughly 85–90 km of the Noto Peninsula coastline and a maximum seaward shoreline advance on the order of 200 m in Minazuki Bay and adjacent sectors of Wajima and Nafune. The magnitude and spatial pattern of the CoastSat–AMBUR shoreline shifts therefore closely match the independently derived ALOS-2 SAR estimates of land emergence and coastline displacement. Small discrepancies between the two products likely reflect differences in shoreline definition, and resolution but both approaches consistently identify the same zones of extreme uplift and new land exposure. Overall, the agreement between the predicted–observed shoreline differencing and the GSI SAR-based deformation maps demonstrates that long-term regression-based shoreline reconstructions, when combined with post-event shoreline extraction, provide a good framework for quantifying earthquake-induced horizontal coastline shifts of about 150–200 m at Wajima and Nafune.

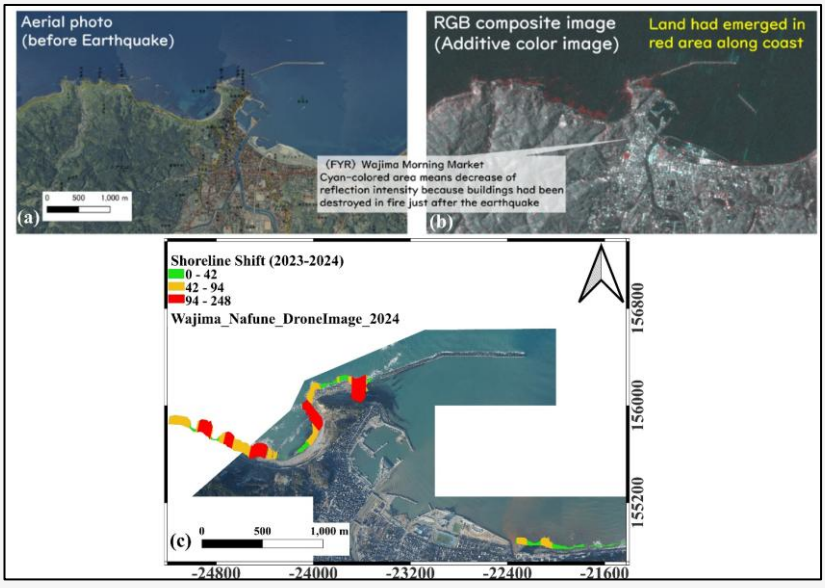

Figure 10: Comparative analysis of CoastSat & AMBUR for pre-and post- earthquake at Wajima: (a) GSI report before earthquake, (b) GSI report after earthquake, and (c) CoastSat & AMBUR shoreline shift pre- and post-earthquake

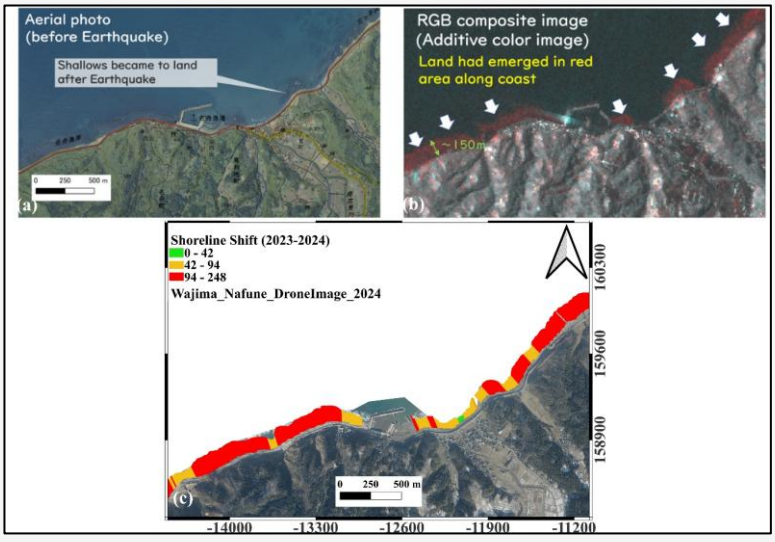

Figure 11: Comparative analysis of CoastSat & AMBUR for pre-and post- earthquake at Nafune: (a) GSI report before earthquake, (b) GSI report after earthquake, and (c) CoastSat & AMBUR shoreline shift pre- and post-earthquake

4. Conclusion

This study evaluated an open-source workflow utilizing satellite data to measure and predict coastline movement across diverse environments. Comprising three primary components shoreline extraction, tidal and water-level correction, and future position prediction the workflow was successfully tested through two distinct case studies. At San Jose Island, Texas, Sentinel-2 shorelines processed via CoastSat were validated against high-accuracy reference data derived from lidar and aerial photography. Following tidal correction, the satellite-derived shorelines aligned closely with reference data in planform view, beach slope, and elevation. Discrepancies were frequently limited to the scale of a single Sentinel-2 10-meter pixel with insignificant overall bias, demonstrating the workflow's reliability. However, larger errors emerged in areas with steep beach slopes or complex geometries, where CoastSat estimates tended to shift further seaward and lower in elevation than the Lidar benchmarks. These limitations stem from applying uniform tidal corrections across the coast rather than tailoring them to individual transects, alongside inherent sensitivities to steep or high-wave-exposure environments. At Wajima, Japan, 28-year Landsat time series successfully predicted pre-earthquake shorelines leading up to the 2024 Noto Peninsula earthquake. Long-term regression models, particularly the Linear Rate of Change (LRR) method achieved sub-pixel accuracy with high R-squared and low MAE values, confirming the efficacy of trend-based modeling. Conversely, these models failed to capture sudden tectonic uplift and subsidence following the 2024 earthquake, resulting in large prediction errors and illustrating that historical trends alone are insufficient during major disruptive events.

Nevertheless, comparing the reconstructed 2023 shoreline with the extracted 2024 post-earthquake shoreline clearly captured the event's impact. The coastlines at Wajima and Nafune advanced seaward by approximately 150–200 meters a magnitude and spatial pattern that strongly corroborate independent SAR-based analyses from the GSI. Overall, this research demonstrates that open-source geospatial tools can deliver reliable multi-decadal shoreline tracking, accurate future predictions, and precise quantification of large, event-driven coastal shifts. Future work will refine tidal corrections by applying them at the individual transect level, expand testing to more complex coastlines, incorporate uncertainty and vertical change estimations, and integrate next-generation altimetry satellites to improve coastal water-level and bathymetry assessments.

Acknowledgments

This research was supported by the Support for Pioneering Research Initiated by the Next Generation (SPRING) Program of the Japan Science and Technology Agency (JST), Grant Number JPMJSP2139, managed by Osaka Metropolitan University (OMU), Osaka, Japan. We also wish to thank the Department of Geosciences OMU for providing a conducive environment for the research, to the supervisors for their guidance and mentorship,

and thanks to all the individuals whose contributions made this study possible.

References

[1] Rahman, M. K., Crawford, T. and Wand Islam, M. S., (2022). Shoreline Change Analysis Along Rivers and Deltas: A Systematic Review and Bibliometric Analysis of the Shoreline Study Literature from 2000 to 2021. *Geosciences*, Vol. 12(11). https://doi.org/10.3390/geosciences12110410.

[2] Kar, P. K., Mohanty, P. K., Pradhan, S., Behera, B., Padhi, S. K. and Mishra, P., (2021). Shoreline Change Along Odisha Coast Using Statistical and Geospatial Techniques. *Journal of Earth System Science*, Vol. 130(209). https://doi.org/10.1007/s12040-021-01703-1.

[3] Ahammed, K. K. B. and Pandey, A. C., (2022). Assessment and Prediction of Shoreline Change Using Multi-Temporal Satellite Data and Geostatistics: A Case Study on the Eastern Coast of India. *Journal of Water and Climate Change*, Vol. 13(3); 1477–1481. https://doi.org/10.2166/wcc.2022.270.

[4] Cenci, L., Disperati, L., Persichillo, M. G., Oliveira, E. R., Alves, F. L. and Phillips, M., (2018). Integrating Remote Sensing and GIS Techniques for Monitoring and Modeling Shoreline Evolution to Support Coastal Risk Management. *GIScience & Remote Sensing*, Vol. 55(3); 355–375. https://doi.org/10.1080/15481603.2017.1376370.

[5] Khurram, S., Pour, A. B., Bagheri, M., Helmy Ariffin, E., Akhir, M. F. and Bahri Hamzah, S., (2025). Satellite-Based Multi-Decadal Shoreline Change Detection by Integrating Deep Learning with DSAS: Eastern and Southern Coastal Regions of Peninsular Malaysia. *Remote Sensing,* Vol. 17(19). https://doi.org/10.3390/rs17193334.

[6] Vitousek, S., Vos, K., Splinter, K. D., Erikson, L. and Barnard, P. L., (2023). A Model Integrating Satellite-Derived Shoreline Observations for Predicting Fine-Scale Shoreline Response to Waves and Sea-Level Rise Across Large Coastal Regions. *Journal of Geophysical Research: Earth Surface*, Vol. 128(7). https://doi.org/10.1029/2022JF006936.

[7] Vos, K., Splinter, K. D., Harley, M. D., Simmons, J. A. and Turner, I. L., (2019). CoastSat: A Google Earth Engine-Enabled Python Toolkit to Extract Shorelines from Publicly Available Satellite Imagery. *Environmental Modelling & Software*, Vol. 122. https://doi.org/10.1016/j.envsoft.2019.104528.

[8] Jackson, C. W. Jr., Alexander, C. R. and Bush, D. M., (2012). Application of the AMBUR R Package for Spatio-Temporal Analysis of Shoreline Change: Jekyll Island, Georgia, USA. *Computers & Geosciences*, Vol. 41, 199–207. https://doi.org/10.1016/j.cageo.2011.08.009.

[9] Morton, R. A. and Pieper, M. J., (1976). Shoreline Changes on Matagorda Island and San Jose Island (Pass Cavallo to Aransas Pass), An Analysis of Historical Changes of the Texas Gulf Shoreline: The University of Texas at Austin, Bureau of Economic Geology, *Geological Circular*, Vol. 42, 76-4. http://dx.doi.org/10.26153/tsw/4972.

[10] Loi, D. H., Jayakody, S., Sassa, K., Konagai, K., Hirota, K., Ono, A., Takanaka, T., Oki, T. and Minamitani, T., (2024). Landslides Triggered by the 2024 Noto Peninsula Earthquake. *Landslides*, Vol. 21, 2583–2590. https://doi.org/10.1007/s10346-024-02333-6.

[11] National Oceanic and Atmospheric Administration. Data Access Viewer. NOAA Digital Coast. [Online]. Available: https://coast.noaa.gov/digitalcoast/tools/dav.html [Accessed: March. 10, 2024].

[12] Geospatial Information Authority of Japan. (2024). Coastline Change Caused by the 2024 Noto Peninsula Earthquake Detected by ALOS-2 SAR Satellite Image. [Online]. Available: https://www.gsi.go.jp/uchusokuchi/uchusokuchi-e31001.html [Accessed: August. 15, 2024].

[13] Long, N., Oanh, N., and Dinh, N. (2025). Application of GIS and Google Earth Engine to Assess Built-up Area Changes during Urbanization in Hai Duong City, Hai Duong Province, Vietnam. *International Journal of Geoinformatics*, Vol. 21(11), 46–58. https://doi.org/10.52939/ijg.v21i11.45993.

[14] Otsu, N., (1979). A Threshold Selection Method from Gray-Level Histograms. *IEEE – Transactions on Systems, Man, and Cybernetics*, Vol. 9(1); 62–66. https://doi.org/10.1109/TSMC.1979.4310076.

[15] Cipolletti, M. P., Delrieux, C. A., Perillo, G. M. E. and Piccolo, M. C., (2012). Superresolution Border Segmentation and Measurement in Remote Sensing Images. *Computers & Geosciences*, Vol. 40; 87–96. https://doi.org/10.1016/j.cageo.2011.07.015.

[16] Lorensen, W. E. and Cline, H. E., (1987). Marching Cubes: A High-Resolution 3D Surface Construction Algorithm. *ACM SIGGRAPH Computer Graphics*, Vol. 21(4); 163–169. https://doi.org/10.1145/37402.37422.

[17] Carrère, L., Lyard, F., Cancet, M., Guillot, A. and Picot, N., (2016). FES 2014, A New Tidal Model Validation Results and Perspectives for Improvements. *Proceedings of the ESA Living Planet Symposium,* 9-13. Prague, Czech Republic: European Space Agency.

[18] Horn, B. K. P., (1981). Hill Shading and the Reflectance Map. *Proceedings of the IEEE*, Vol. 69(1); 14-47. https://doi.org/10.1109/PROC.1981.11918.

[19] Cong, P., Evans, C., MacInnis, B., Czenze, A., Mehlmann, M., Sutherland, M., Whidden, C. and Morrison, L., (2026). Adapting the COASTGUARD Shoreline Detection Workflow to Macrotidal Estuaries: A Case Study in the Musquash Estuary Marine Protected Area. *Frontiers in Marine Science,* Vol. 13. https://doi.org/10.3389/fmars.2026.1796587.

[20] O'Neill, A. C., Batiste, S. F., Buscombe, D. D., Burgess, J., Doran, K. S., Gibbs, A. E., Henderson, R. E., Heslin, J. L., Janda, C. N., Lundine, M. A., Terrano, J. F., Warrick, J. A. and Weber, K. M., (2025). Comparisons of Shoreline Positions from Satellite-Derived and Traditional Field- and Remote-Sensing Techniques, *Open-File Report 2025–1054*, Vol. 41. https://doi.org/10.3133/ofr20251054.

[21] Harrys, R. M., (2024). rifqiharrys/sdb_gui: SDB GUI 3.6.1 (v3.6.1) [Software]. Zenodo. https://doi.org/10.5281/zenodo.11045690.

[22] Dolan, R., Fenster, S. M and Holme, J. S., (1991). Temporal Analysis of Shoreline Recession and Accretion. *Journal of Coastal Research*, Vol. 7(3); 723–744. http://www.jstor.org/stable/4297888.

[23] Thieler, E. R. and Danforth, W. W., (1994). Historical Shoreline Mapping (I): Improving Techniques and Reducing Positioning Errors. *Journal of Coastal Research,* Vol. 10(3); 549–63. http://www.jstor.org/stable/4298252.

[24] Fenster, S. M., Dolan, R. and Elder, J. F., (1993). A New Method for Predicting Shoreline Positions from Historical Data. *Journal of Coastal Research*, Vol. 9(1); 147–171. http://www.jstor.org/stable/4298075.

[25] Crowell, M., Douglas, B. C. and Leatherman, S. P., (1997). On Forecasting Future U.S. Shoreline Positions: A Test of Algorithms. *Journal of Coastal Research*, Vol. 13(4); 1245–1255. http://www.jstor.org/stable/4298734.

[26] Frazer, L. N., Genz, A. S. and Fletcher, C. H., (2009(a)). Toward Parsimony in Shoreline Change Prediction I: Basis Function Methods. *Journal of Coastal Research*, Vol 25(2); 366–379. https://doi.org/10.2112/06-0756.1.

[27] Frazer, L. N., Anderson, T. R. and Fletcher, C. H., (2009b). Modeling Storms Improves Estimates of Long-Term Shoreline Change. *Geophysical Research Letters*, Vol. 36(20). https://doi.org/10.1029/2009GL040061.

[28] Genz, A. S., Frazer, L. N. and Fletcher, C. H., (2009). Toward Parsimony in Shoreline Change Prediction (II): Applying Basis Function Methods to Real and Synthetic Data. *Journal of Coastal Research*, Vol. 25(2); 380–392. http://www.jstor.org/stable/27698330.